Journal Pre-proof

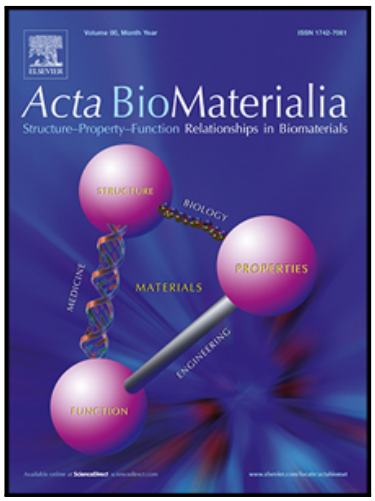

Toward a disruptive, minimally invasive small finger joint implant concept: Cellular and molecular interactions with materials in vivo

Heithem Ben Amara , Pardis Farjam , Theresa M. Lutz , Omar Omar , Anders Palmquist , Oliver Lieleg , Martin Browne , Andy Taylor , Gijsbertus J. Verkerke , Jeroen Rouwkema , Peter Thomsen

PII: S1742-7061(24)00289-7
DOI: https://doi.org/10.1016/j.actbio.2024.05.042
Reference: ACTBIO 9344

To appear in: *Acta Biomaterialia*

Received date: 23 January 2024
Revised date: 21 May 2024
Accepted date: 24 May 2024

Please cite this article as: Heithem Ben Amara , Pardis Farjam , Theresa M. Lutz , Omar Omar , Anders Palmquist , Oliver Lieleg , Martin Browne , Andy Taylor , Gijsbertus J. Verkerke , Jeroen Rouwkema , Peter Thomsen , Toward a disruptive, minimally invasive small finger joint implant concept: Cellular and molecular interactions with materials in vivo, *Acta Biomaterialia* (2024), doi: https://doi.org/10.1016/j.actbio.2024.05.042

Toward a disruptive, minimally invasive small finger joint implant concept: Cellular and molecular interactions with materials *in vivo*

Authors

Heithem Ben Amara[1]#, Pardis Farjam[2]#, Theresa M. Lutz[3], Omar Omar[4], Anders Palmquist[1], Oliver Lieleg[3], Martin Browne[5], Andy Taylor[6], Gijsbertus J. Verkerke[2], Jeroen Rouwkema[2], Peter Thomsen[1]*

Affiliations

[1] Department of Biomaterials, Institute of Clinical Sciences, Sahlgrenska Academy, University of Gothenburg, Sweden.

[2] Department of Biomechanical Engineering, Faculty of Engineering Technology, University of Twente, Enschede, the Netherlands.

[3] School of Engineering and Design, Department of Materials Engineering, Technical University of Munich, Munich, Germany.

[4] Department of Biomedical Dental Sciences, College of Dentistry, Imam Abdulrahman bin Faisal University, Dammam, Saudi Arabia.

[5] Bioengineering Science Research Group, School of Engineering, University of Southampton, Southampton, UK.

[6] Aurora Medical Ltd, Chichester, UK.

#Equal contribution

***Corresponding author:**

Peter Thomsen

Department of Biomaterials, Institute of Clinical Sciences

Sahlgrenska Academy, University of Gothenburg

E-mail: peter.thomsen@biomaterials.gu.se

Box 412; SE-405 30

Gothenburg, Sweden.

Abstract

Osteoarthritis (OA) poses significant therapeutic challenges, particularly OA that affects the hand. Currently available treatment strategies are often limited in terms of their efficacy in managing pain, regulating invasiveness, and restoring joint function. The APRICOT® implant system developed by Aurora Medical Ltd (Chichester, UK) introduces a minimally invasive, bone-conserving approach for treating hand OA (https://apricot-project.eu/). By utilizing polycarbonate urethane (PCU), this implant incorporates a caterpillar track-inspired design to promote the restoration of natural movement to the

joint. Surface modifications of PCU have been proposed for the biological fixation of the implant. This study investigated the biocompatibility of PCU alone or in combination with two surface modifications, namely dopamine-carboxymethylcellulose (dCMC) and calcium-phosphate (CaP) coatings. In a rat soft tissue model, native and CaP-coated PCU foils did not increase cellular migration or cytotoxicity at the implant–soft tissue interface after 3 d, showing gene expression of proinflammatory cytokines similar to that in non-implanted sham sites. However, dCMC induced an amplified initial inflammatory response that was characterized by increased chemotaxis and cytotoxicity, as well as pronounced gene activation of proinflammatory macrophages and neoangiogenesis. By 21 d, inflammation subsided in all the groups, allowing for implant encapsulation. In a rat bone model, 6 d and 28 d after release of the periosteum, all implant types were adapted to the bone surface with a surrounding fibrous capsule and no protracted inflammatory response was observed. These findings demonstrated the biocompatibility of native and CaP-coated PCU foils as components of APRICOT® implants.

Keywords

Animal models, Biocompatibility, Gene expression, Osteoarthritis, Polyurethanes

1. Introduction

Among joint diseases, osteoarthritis (OA) is the predominant cause of disability (*1*), with the hand being one of the most commonly affected areas (*2*). Hand OA is characterized by inflammation-driven articular cartilage degradation and bone remodeling, frequently leading to significant pain and limitation of movement (*3*). Due to the considerable morbidity that is associated with OA, extensive efforts have focused on the development of pharmacological treatments (*4*, *5*) primarily aimed at alleviating pain and mitigating cartilage damage (*6*). However, these interventions often fail to stop disease progression, making surgical intervention an inevitable choice in advanced stages of hand OA (*7*).

Arthroplasty of the hand, which involves the surgical removal and replacement of damaged cartilaginous surfaces in the joint, is often the only option for improving mobility and alleviating pain for many patients (*7*). This approach typically requires the use of an implant (*8*), and it particularly involves the proximal interphalangeal (PIP), metacarpophalangeal (MCP), and trapeziometacarpal (TMC) joints (*9*). Historically, hinged silicone prostheses (*10*) have been used as a mainstay for hand arthroplasty, primarily facilitating joint spacing (*11*). Despite being considered the gold standard, these implants are associated with complications such as deformity correction issues, implant fractures, and

synovitis (*9*). Subsequent developments in implant materials, including metal-on-plastic and pyrolytic carbon, have offered some improvements. However, limitations in motion, joint instability, recurrent pain, and concerns about implant longevity and reoperation rates continue to limit the efficacy of these treatments (*12*).

Despite its long history, hand arthroplasty has not achieved the same level of success as hip or knee arthroplasty (*13*), with complication rates as high as 35% (*14*). In fact, the transfer of hip and knee arthroplasty technologies to hand joints often overlooks the unique characteristics of hand joints: their small size, variable loading, involvement in kinetic chains, extensive range of movement, and intricate soft tissue structures (*15*). Achieving implant stability in hand arthroplasty typically requires techniques such as intramedullary, press-fit, bone ingrowth, or cemented fixation (*15*), which increases the invasiveness of the procedure. As a result, innovative approaches that minimize tissue damage, enhance range of motion, and effectively alleviate pain during the treatment of hand OA are increasingly needed.

The APRICOT® (Anatomically Precise Revolutionary Implant for Conserving Osteoarthritis Treatment) system provides an implant design (*16*) for minimally invasive hand OA surgery (**Figure 1**). APRICOT® avoids the need to remove bone and simplifies implant insertion and removal, significantly reducing the requirement for general anesthesia and extensive surgical procedures. The implant utilizes thin foils of polycarbonate urethane (PCU), a polyurethane elastomer that is known for its biostability, wear resistance, and a balance of toughness and compliance, making it a suitable candidate for use in orthopedic joint implants. For example, PCU has demonstrated efficacy for knee hemiarthroplasty and total meniscus replacement (*17*). The innovative design of APRICOT®, inspired by caterpillar track movement, prevents sliding at joint surfaces, thus reducing wear and tear at the implant site. By avoiding the articulation of two solid components typical of conventional implants, the APRICOT® design confines any wear debris within the implant, mitigating potential damage. Minimally invasive fixation systems (*18*) that utilize either biological glues or mechanical fixation, in addition to surface functionalization protocols, are vital for ensuring ultralow friction and smooth joint movement of APRICOT® implants.

As a whole joint disease, OA affects the articular cartilage, subchondral bone, ligaments, the capsule, synovium, and periarticular muscles (*19*). Central to the APRICOT® concept is minimizing the activation of inflammation and the associated reparative response in all joint components, including both soft tissue and bone. Ensuring the biocompatibility of the implant via the characterization of the local cellular and molecular inflammation and tissue repair mechanisms is crucial. Such an understanding is even more important considering that inflammation is a key driver of OA progression.

The present study aimed to investigate the cellular and molecular responses to PCU implants in soft tissue and their ability to adapt to bone without causing protracted inflammation. PCU foils, were tested alone or in combination with two candidates for surface modification: a dopamine-based bioadhesive film [dopamine-carboxymethylcellulose (dCMC) conjugate] and a calcium-phosphate (CaP) coating. While the use of dCMC is aimed at forming molecular bonds with tissue surfaces through carboxyl groups of carboxymethylcellulose (*20*) and the catechol functional groups of dopamine, the CaP coating is designed to encourage bone ingrowth to promote implant stability (*21*). Employing dedicated soft tissue (*22-24*) and bone models in rats, the present study demonstrated that PCU implants do not exacerbate initial inflammation, except when PCU implants were combined with dCMC films which exhibit early cytotoxicity in soft tissue. Finally, the placement of PCU implants on bone surfaces after the release of the periosteum resulted in effective mitigation of inflammation and adaptation of the implants to the bone via a fibrous encapsulation.

2. Materials and methods

2.1. Implants

Discs (diameter = 10 mm; thickness = 300 μm) and rectangular membranes (3 mm x 6 mm; thickness = 200 μm) were made from bare polycarbonate urethane (PCU) alone, a polycarbonate urethane–dopamine-carboxymethyl cellulose composite (dCMC), and polycarbonate urethane coated with calcium phosphate (CaP).

2.1.1. **PCU:** PCU implants were manufactured from polycarbonate (PCU) film that was extruded from pellets (Carbothane AC-4085 A, Aurora Medical Ltd) using a fully representative manufacturing process by Aurora Medical Ltd. The discs and rectangular membranes were cut under identical temperature, vacuum profiles and forming strains, prior to washing (70% EtOH and diH_2O, in sequence) and drying.

2.1.2. **dCMC**: d-CMC adhesive films were developed at the Technical University of Munich by employing carbodiimide chemistry to create d-CMC conjugates. Carboxymethylcellulose molecules (Biosynth Carbosynth; YC44523; viscosity 1.000–1.300 mPa/s) were dissolved in 2-(N-morpholino)ethanesulfonic acid [MES; 1% (w/v); 10 mM; pH = 5] prior to a 3-h incubation with 1-ethyl-3-(3-dimethylaminopropyl)carbodiimide (EDC, Carl Roth; 5 mM) and N-hydroxysulfosuccinimide (sulfo-NHS, abcr GmbH, 5 mM). The solution was then mixed (1:1) with dopamine hydrochloride [1 % (w/v), Sigma Aldrich] in phosphate-buffered saline (PBS), incubated with shaking (overnight; 4°C), and dialyzed against ultrapure water (48 h; 4°C). After the solution was frozen and lyophilized for 2 d, the obtained dCMC powder was solubilized in water (10 mg/mL) and poured into custom-made polycarbonate 6-well plates prior to degassing under a vacuum to obtain films that were subsequently dried (48 h; room temperature).

2.1.3. **CaP**: For coating with calcium-phosphate, cleaned PCU samples were exposed to cold low-pressure oxygen plasma (40 s; 0.5 Torr; 50 W) using a plasma cleaner (CUTE, Femto Science). Each sample was then immediately transferred to a 48-well plate and vertically suspended for 24 h in supersaturated simulated body fluid (SBF; 1 mL/well; 37°C) followed by washing (diH_2O) and drying (N_2) as previously described (*21*).

2.2. Preimplantation characterization

Surface microstructure of PCU and CaP implants were examined using a scanning electron microscope (SEM, JEOL JSM-IT 100) following gold sputter-coating (10 mA, 60 s). The chemical characterization of CaP and PCU was performed using X-ray diffraction (XRD, D8 DISCOVER, Bruker). Crystallography Open Database (COD) and Mercury 4.0 software were used to analyse the data. The percentage of crystallinity was computed using DIFFRAC.EVA software (v 4.3.1.2). In addition, the degree of dopamine functionalization in dCMC was assessed by determining the absorption behaviour of the different molecular solutions (CMC, dCMC, dopamine) at a 250-350 nm wavelength range (SpectraMax ABS Plus, Molecular Devices) using solutions of 10 mg mL^{-1} in ddH_2O each. From the obtained data, the degree of functionalization of CMC with dopamine was calculated.

2.3. Animal models and surgical procedures

Female Sprague–Dawley rats (250–300 g; Taconic Biosciences) were used for the *in vivo* testing of disc-shaped implants in soft tissue (n = 24) and of membranes in bone (n = 46). These experiments were approved by the Local Ethical Committee for Laboratory Animals at the University of Gothenburg, Sweden (*soft tissue experiments*: Dnr-4725/2023; *bone experiments*: Dnr-14790/2019).
The soft tissue model (*22-24*) allows investigation of cellular responses in three topographically distinct compartments of the implant–soft tissue interface: ***i)*** the cells adherent to the implant surface, ***ii)*** the inflammatory fluid around the implant (*exudate*), and ***iii)*** the peri-implant soft tissue. In brief, surgeries were carried out under anesthesia induced by 4% isoflurane inhalation. The backs of the rats were shaved and cleaned before eight separate incisions were made to form subcutaneous pockets via blunt dissection. In each rat, six experimental sites received disc-shaped implants (PCU, CaP, and dCMC) and two were left without implants (n = 2, Sham) before closure with nonresorbable sutures. After cleaning of their backs, the rats were recovered from anesthesia and returned to the animal facility. Temgesic (Reckitt Benckiser; 0.03 mg/kg) was administrated for analgesia immediately and at 8 h post-surgery. The rats were euthanized with an overdose of pentobarbital after 3 d or 21 d (n = 12/timepoint), and three types of samples were collected: ***i) implants*** (n = 8/group/time point***):*** implants were collected following pocket re-entry for analyses of adherent cells (counting or gene expression); ***ii) peri-implant exudate*** (n = 8/group/time point***):*** exudate was obtained from the pockets by lavage with PBS following implant retrieval, and each retrieved volume was divided to

analyze cells (counting, viability, cytotoxicity, or gene expression***)***; ***iii) implant and peri-implant tissue*** (n = 8/group/time point***):*** tissues were dissected *en bloc* for histology and histomorphometry.

The bone model enables the study of membrane adaptation to bone. In brief, the rats were anesthetized with 4% isoflurane, followed by shaving and cleaning of the surgical sites on both hind limbs, and local complementary anesthesia by administration of lidocaine. Incision and reflection of the skin and muscle were then performed, followed by periosteum release to expose the metaphyses to the tibiae. Based on a predefined randomization scheme, the exposed bone surface in each tibia of all rats was implanted with one membrane (PCU, CaP, or dCMC) or was left without implants (Sham). Mattress sutures stabilized the membranes to the surrounding periosteum and soft tissues, followed by the repositioning of the overlaying muscles and skin, and Temgesic-analgesia was induced immediately and at 8 h post-surgery. The rats were euthanized after 6 d and 28 d (n = 24/timepoint), and the implants and associated soft and bone tissues were subjected to *en bloc* dissection (n = 8/group/timepoint) for histology, histomorphometry, and immunohistochemistry.

2.4. Cell counting, cell viability, and cytotoxicity

Implants and exudates that were collected from the soft tissue pockets at 3 d and 21 d were used to quantify the number of cells that adhered to the implant (n = 8/group/time point) and the number of cells that was present in the exudate (n = 8/group/time point) using the NucleoCounter® system (ChemoMetec). For the counting of implant-adherent cells, the collected implants were immediately submerged in a lysis buffer (100 µL, Reagent A100, ChemoMetec) in a 96-well plate and shaken (2 min, 500RPM) to facilitate cell detachment. A stabilization buffer was added to the cell lysate (100 µL, Reagent B, ChemoMetec) prior to loading into a NucleoCassette™ with propidium iodide to stain the nuclei; then the total number of cells was automatically counted. To count the number of cells present in the exudate, an exudate fraction was directly introduced into a NucleoCassette™ to count the dead cells. Additionally, another fraction of the exudate was diluted at a 1:1:1 ratio with the lysis and stabilization buffers and then loaded into a NucleoCassette™ to count the total number of cells. Moreover, to assess cytotoxicity, dedicated exudate volumes (110 µL; n = 8/group/time point) were centrifuged to quantify lactate dehydrogenase (LDH) levels through the spectrophotometric measurement of lactic acid which is a product of the LDH-mediated pyruvic acid conversion (C-laboratory, Sahlgrenska University Hospital, Gothenburg).

2.5. Gene expression

Quantitative polymerase chain reaction (qPCR) was conducted on cells from two different compartments of the soft tissue pockets: ***i) exudate*** (n = 8/group/time point): after removing an exudate fraction for cell counting, the remaining exudate volume was centrifuged (400 × g, 5 min) to pellet the cells which were lysed in RNA Shield (Zymo Research), and ***ii) implant surface*** (n = 8/group/time point): retrieved implants were placed in RNA Shield to lyse the adherent cells. Cell

lysates from the exudates and from the implant surfaces were subsequently frozen (-80°C). RNA extraction was performed using an RNeasy Micro Kit (Qiagen GmbH), according to the manufacturer's guidelines. RNA integrity and concentration were assessed in a preliminary pilot study using a Pico 6000 RNA Kit (Bioanalyzer 2100 system, Agilent Technologies) and a Nanophotometer P-36 (Implen GmbH), respectively. cDNA synthesis was performed using the TATAA GrandMaster cDNA Synthesis Kit (TATAA Biocenter AB), following the prescribed protocols. Previously validated primers (Bio-Rad) were used for the gene panel listed in **Table S1**. The reference gene panel included the following rat genes: 18s, ACTB, GAPDH, HPRT1, YWHAZ (Bio-Rad) and gene stability was determined by GeNorm and Normfinder (GenEx software, Multid). HPRT1, which was identified as the most stable, was used for normalization. Relative gene expression was calculated using the delta-delta-Cq method.

2.6. Histology

Implants and adjacent tissues that were obtained from both soft tissue and bone experiments were preserved in formalin, decalcification (of bone samples only) in Ethylenediaminetetraacetic acid (EDTA; 10%) followed by dehydration and paraffin infiltration. Tissue sections were cut at a thickness of 5 µm (Leica RM 2255, Leica Biosystems Nussloch GmbH), deparaffinized with xylene, stained with hematoxylin and eosin, and examined using an optical microscope (Nikon Eclipse E600, Nikon).

2.7. Immunohistochemistry, TRAP staining, and TUNEL staining

Immunohistochemistry was performed on sections from the soft tissue and bone experiments. Tissue sections were deparaffinized, rehydrated, and washed in PBS. Antigen retrieval was achieved by incubating the sections at 90°C for 20 min, followed by blocking with a 5% solution of goat serum in 4% bovine serum for 30 min. Primary rabbit polyclonal antibodies targeting iNOS (PA1036, Thermo Fisher), MRC1 (PA5101657, Thermo Fisher), and Periostin (PA5-79850, Thermo Fisher) and CD68 (PA581594, Thermo Fisher) were added at dilutions of 1:100, 1:30, 1:100, and 1:1500 respectively, and incubated for 2 h at room temperature. Immunoreactivity was detected using the Pierce Horseradish Peroxidase detection system (Thermo Fisher) with DAB (Metal Enhanced DAB Substrate Kit, Thermo Fisher) as the chromogen, following the manufacturer's protocols. Control sections were processed similarly, excluding the primary antibodies, and served as negative controls. In addition, selected sections from the soft tissue experiments were stained with the TUNEL Assay-Kit (ab206386, Abcam) to detect apoptotic cells, according to the manufacturer’s protocol. Similarly, selected sections from the bone experiments were subjected to TRAP staining (387A-1KT, Sigma-Aldrich) to detect osteoclasts, following the manufacturer’s instructions.

2.8. Image analysis

Full digital scans of the soft tissue and bone sections were captured using a Plan Apo 20x/0.5 objective lens mounted on an optical microscope. Images were imported into QuPath v.0.4.3 software for histomorphometric analysis of peri-implant tissues.

For soft tissues, the 21-d peri-implant fibrous capsules (n = 4/group/timepoint) were evaluated using the following parameters: ***i) thickness of the fibrous capsule***: was measured using 20 equidistant lines, ***i) area of the fibrous capsule:*** was measured by manually outlining the fibrous capsule using the '*wand tool'* and normalizing this measurement to the fibrous capsule perimeter, and ***iii) cell density of the fibrous capsule:*** was calculated using automatic cell nuclei detection ('*Cell detection'* plugin) and normalized to the capsule area. This cell density was compared to that in the subcutaneous fascia at Sham sites (within a rectangular region of interest matching the average fibrous capsule area around all implants i.e., ~ 650 000 μm^2).

For bone, cell density was measured in tissues surrounding the implants within a distance of 100 μm from the implant-tissue interface and normalized to the area of the defined region of interest. The cell density of the peri-implant tissues was compared to that of the soft tissue overlaying cortical bone of Sham sites. The region of interest in the Sham group had a rectangular shape and an area equal to the average area of all peri-implant regions of interest, i.e., ~ 400 000 μm^2. In addition, identical regions of interest in immunohistochemistry sections from bone-implanted tissues were used to quantify cells positive to iNOS, MRC1, and Periostin. For this purpose, scans of the implants and peri-implant tissues or of sham-operated tissues were transferred to QuPath v.0.4.3 software and cells were counted using the automated 'positive cell detection' plugin. The proportion of positive cells was measured in an average of ~1600 cells/region of interest.

2.9. Statistical analysis

Statistical comparisons of cell counts, cytotoxicity, and histomorphometric parameters were performed using the unpaired Kruskal–Wallis U test. Statistical comparisons of the gene expression data were performed using two-way ANOVA with multiple comparisons via test Benjamini and Hochberg's test of the false discovery rate. Differences for which $P < 0.05$ were considered statistically significant.

3. Results

3.1. Preimplantation characterization

The surfaces of PCU and CaP were examined using SEM (**Figure 2a)**. CaP showed a uniform homogenous multi-layer coating with a thickness of 5.8 μm as reported elsewhere (*21*)**.** The general structure of the coating consisted of a dense layer with a porous surface, including micro-cracks that were covered with porous globules (**Figure 2a)**. The stability of CaP coating on the PCU surface was previously evaluated with a scratch test and a 180° bend test (*21*). The scratch test showed that the coating did not delaminate up to a shear stress of 16.9 (±4) MPa. The bend test demonstrated that the

coating remained stable, with only limited propagation of existing small cracks, upon severe deformation of the flexible PCU substrate (*21*). The crystal structure of PCU and CaP was determined by XRD (**Figure 2b)**. CaP implants did not reveal any peaks of bare PCU. An amorphous halo was detected for CaP with the calculated crystallinity index (CrI) of 27.7%. The well-developed discrete peaks were visible at 2Θ=12.1 ° and 2Θ=23.9 °, and small peaks at 2Θ=29.8 °, 2Θ=32.11 °, 2Θ=45.8 °, and 2Θ=48.4 ° which revealed similarities with Brushite crystal structures. The dCMC was based on carboxymethyl-cellulose modified by dopamine molecules. Spectroscopic analysis (**Figure 2c)** showed a pronounced peak at 280 nm, which is typical for the dopamine molecule. From the peak height, the degree of catechol functionalization achieved with the chemical coupling procedure was calculated as 43 %.

3.2. Implants in soft tissue elicit a transient cellular migration and a transient upregulation of inflammatory cytokines and chemokines

To study the cellular and molecular responses to the implants, the cells adherent to the implant surface and those in the inflammatory fluid around the implant (exudate) were retrieved from the subcutaneous pockets (**Figure 3a-f)**.

Samples were harvested at postoperative days 3 and 21 which enabled the investigation of initial inflammation and subsequent tissue repair and regeneration, respectively. All the experimental sites remained closed and did not feature clinically discernible macroscopic signs of dermal inflammation**.**

The number of cells that were present in the exudate (**Figure 3g)** or adhered to the implants (**Figure 3h)** at 3 d were higher than those observed at 21 d across all groups, demonstrating a transient, acute inflammatory response attributable to the synergistic influence of surgical intervention and the implant. No difference in the number of cells at the surface of the different implant types or in the exudates, or in the ratio of the number of implant adherent cells to the number of exudate cells (**Figure 3i)** were observed at either timepoints. Cell counts in the per-implant exudate did not differ from Sham exudates at 3 d. Such a comparison was not feasible after 21 d owing to the natural healing process at the Sham sites, resulting in the absence of a detectable pocket after 21 d.

qPCR (**Figure 3j)** was performed to study the gene expression of critical inflammatory cellular mediators and chemoattractants such as cytokines (*TNF* and *IL8)* and chemokines (*IL8* and *MCP1).* A modest increase in the expression of proinflammatory cytokines was evident at 3 d. Among the groups, the dCMC group exhibited a more robust *TNF* gene response in both cells within the exudate and those adherent to the implant surface. Importantly, the expression levels of the potent chemoattractants *IL8* and *MCP1* exhibited a significant decline from 3 d to 21 d, highlighting the transient nature of the initial inflammatory response to the implants.

Overall, all the implants resulted in a transient increase in cell infiltration and the expression of inflammatory cytokine and chemokine genes. This response was particularly noticeable in the dCMC group.

3.3. The dCMC coating transiently potentiates the initial inflammatory response and activates proinflammatory macrophage polarization pathways

Histology was performed to examine the soft tissues that interfaced with the implants and Sham pockets. At 3 d (**Figure 4a**), the fascial loose connective tissue, which is situated beneath the subcutaneous musculature surrounding all the implants, exhibited an evident infiltration of inflammatory cells in comparison to the wounded subcutaneous facia in Sham sites. This inflammatory infiltration, which suggested pronounced cellular recruitment, was also observed close to the tissue interface with the implants where a proteinaceous network was particularly visible. Also detectable around blood vessels irrigating the subcutaneous fascia, the cellular infiltrates consisted mostly of mononuclear cells and polymorphonuclear leukocytes and appeared denser in the dCMC group than in the other groups (**Figure 4a**).

qPCR analysis of cells that were present in the exudate or those adherent to the implants was performed to study of the expression of genes encoding for macrophage markers (**Figure 4b**). Macrophages are key for orchestrating the reparative/regenerative response to biomaterials, and play different roles during inflammation and tissue repair.

The expression of *iNOS*, which is a marker of the M1 macrophage phenotype crucial during the initial inflammatory phase, decreased from 3 d to 21 d both in cells that were present in peri-implant exudates or those adherent to the implants. Notably, the dCMC group exhibited the highest expression of *iNOS* at 3 d, exceeding the expression of this gene in exudate cells and implant-adherent cells in the other groups by more than 4-fold and 6-fold, respectively. This marked increase was transient and was not observed at 21 d. In contrast, no differences in *iNOS* mRNA levels were detected between PCU, CaP, or Sham at either timepoints.

Furthermore, qPCR was used to analyze the expression of *ARG1*, *MRC1*, and *IL10*, genes associated with the M2 macrophage phenotype that is pivotal during tissue repair and regeneration. Specifically, in cells adherent to dCMC implants, the gene expression of *ARG1* and *IL10*—but not *MRC1*—was higher than that of the PCU and CaP groups at 3 d, and then decreased to comparable levels across all groups at 21 d. In exudate cells, the gene expression of *MRC1*—but not *ARG1* and *IL10*—were lower in dCMC group than that in the PCU, CaP, and Sham at 3 d, and then increased to a similar level as that in the other groups at 21 d. Importantly, the ratios *iNOS/ARG1* (**Figure 4c, Figure S1a-b**) and *iNOS/MRC1* (**Figure S1c-d**) ratios were 2- to 100-fold higher in the dCMC group than that in the other groups at 3 d, further illustrating the strong activation of M1 macrophage-related pathways by dCMC. This trend remained at 21 d but at a considerably lower amplitude, confirming the transient nature of the initial proinflammatory response of macrophages that was induced by dCMC. Moreover,

immunohistochemistry targeting the proinflammatory macrophage marker CD68 in soft tissue sections (**Figure 4d**) showed an evident presence of positive cells at 3 d, particularly t the vicinity of the dCMC-coated implants. At 21 d, only a few CD68-positive cells were detected (**Figure S4**).

In summary, the gene and protein expression of macrophage markers was comparable among PCU, CaP, and Sham groups. dCMC resulted in the establishment of an initial proinflammatory milieu that was characterized by cellular infiltration into the peri-implant soft tissues and potent upregulation of M1 macrophage-related gene and protein expression. This inflammatory phase was succeeded by a transition toward the induction of M2 macrophage-related gene expression, indicative of a shift to reparative mechanisms.

3.4. dCMC but not by PCU or CaP elicits increased initial cytotoxicity

Cell death plays a critical role in inflammation and tissue repair/regeneration. Cell viability and cytotoxicity were therefore quantified in the exudates through analysis of dead cells (**Figure 5a)**, and measurements of the extracellular release of lactate dehydrogenase (LDH, **Figure 5b**), which is an enzyme released upon the cytoplasmic membrane disruption.

At 3 d, the number of dead cells in the exudate was elevated across all groups. The dCMC group exhibited the highest number of dead cells. This finding was consistent with the concentration of LDH which was the highest in the dCMC group at 3d.

At 21 d, the number of dead cells decreased in all groups. LDH concentration did not vary between 3 d and 21 d, except in the PCU group which exhibited an increase in LDH levels over time.

Furthermore, apoptosis-related pathways were studied by qPCR analysis (**Figure 5c**) of the expression of proapoptotic (*DDIT4* and *CASP3*) and antiapoptotic (*BCL2*) genes. At 3 d, the dCMC group exhibited an elevated expression of proapoptotic genes *DDIT4* and *CASP3* particularly in implant-adherent cells; these results confirmed dead cell count and cytotoxicity findings. The *DDIT4/BCL2* ratio further showed clear induction of apoptosis gene expression in the dCMC group at 3 d (**Figure 5d; Figure S2**). At 21 d, both proapoptotic and antiapoptotic genes exhibited overall higher expression compared to 3 d in cells from exudates or in cells adherent to the implants. In addition, TUNEL staining revealed a notable presence of apoptotic in soft tissues at 3 d especially close to the interface with the dCMC-coated implants (**Figure 5d**). Only a few TUNEL-positive cells were observed in tissues at 21 d (**Figure S5**).

Taken together, these findings indicate that, at 3 d, dCMC induced increased cell death and cytotoxicity as well as the induction of apoptosis-related gene expression.

3.5. PCU implants foster fibrous encapsulation

To determine whether the differential regulation of inflammation and apoptosis-related pathways affected tissue repair/and regeneration, qPCR analysis of the expression of selected proregenerative

(*FGF2*, *COL1A1*, and *TGFβ*) and neoangiogenetic (*VEGF*) markers was performed (**Figure 6a**). mRNA levels of these genes noticeably increased between 3 d and 21 d, regardless of the group or whether the cells were harvested from the exudate or from the implant surface. At 3 d, dCMC increased the expression of *VEGF* gene, which was evident in cells adherent to the implants, but decreased the expression of the proregenerative gene *COL1A1* in cells from the exudates. In contrast, PCU activated fibrogenesis pathways as early as 3 d by upregulating the *TGFβ* gene. At 21 d, the highest *COL1A1* gene expression was observed in cells from exudates in the CaP group.

Histology was performed at 21 d (**Figure 6b**) to verify whether the differential regulation of proregenerative genes led to morphological differences in the fibrous encapsulation of the implants. All the implants were encircled with a 50-100-µm-thick fibrous capsule with a dense fibrillar content that was preferentially oriented in parallel to the implant surface and in which cells and blood vessels were visible. The PCU group had the thickest fibrous capsule (**Figure 6c**). The cell infiltration of the tissue surrounding the implants markedly decreased between 3 d and 21 d. The density of cells in the 21-d peri-implant fibrous capsule was comparable among PCU, dCMC, and CaP groups, but higher than the density of cells in the 21-d subcutaneous fasciae of Sham sites (**Figure 6c**; **Figure S3)**.

To summarize, while dCMC increased gene expression related to neoangiogenesis, PCU resulted in an early activation of fibrogenesis genes, fostering implant encapsulation.

3.6. dCMC and CaP do not alter the regulation of cellular adhesion-related genes

Considering the potential adhesive properties of dCMC and CaP, the expression of cellular receptors that are involved in cellular adhesion in the initial stage of inflammation (*TLR4*) or in the subsequent reparative phase (*ITGβ1* and *ITGβ2*) was studied by qPCR analysis (**Figure 7**). *TLR4* gene expression was elevated at 3 d in the dCMC group but substantially decreased over time in all the groups, suggesting the attenuation of inflammation over time in response to the implants. A contrasting trend was observed in the expression of the integrin genes *ITGβ1* and *ITGβ2*. Across all the groups, both genes were more highly expressed at 21 d than at 3 d, but there were no noticeable differences between the different implants.

3.7. PCU, dCMC and CaP are adapted to the bone surface via fibrous encapsulation

To study the interaction between bone and the implants (PCU, dCMC or CaP), with Sham sites serving as a control, the implants were placed on a flat bone surface, denuded of periosteum, on the proximal metaphyses of tibiae in rats (**Figure 8a-g)**.

At 6 d and 28 d, all the experimental sites remained closed and did not feature clinically discernible macroscopic signs of inflammation in the skin. Throughout the observation period, none of the animals featured gait impairment attributable to the surgical procedure or the presence of the implants. The implants with the surrounding tissues were coronally cut (**Figure 8g**). The histological sections

were used to visualize the implanted membranes, the underlying bone, and the adjacent soft tissues (**Figure 8h**).

At 6 d (**Figure 8i, k**), cellular infiltration into the connective tissue surrounding the implant was evident in all the experimental groups. The infiltrating cells consisted mostly of mononuclear cells and were surrounded by an abundant extracellular matrix with numerous small blood vessels, which is typical of granulation tissue. The connective tissue interposed between the implants and bone exhibited less pronounced cellular infiltration than that in the connective tissue overlying the implants.

At 28 d (**Figure 8j, k**), all implants were consistently surrounded by a dense fibrillar capsule that was sporadically interrupted by direct contact between the implants and the underlying bone. Of all the examined specimens (n=30 at 6 d; n=30 at 28 d), bone–implant contact was observed only in one PCU at 28 d, not exceeding 0.8%. In contrast, at 6 d, the density of cells was comparable between the top and bottom areas of the connective tissue surrounding the implants.

Histomorphometry (**Figure 8l**) was performed in a region of interest around the implants within 100 μm from the implant-tissue interface, and demonstrated comparable cellular density across all groups at 6 d and 28 d. No differences were found with respect to cell infiltration between the test sites and Sham sites.

Immunohistochemistry was executed to determine the presence of cells expressing the iNOS (inducible nitric oxide synthase, **Figure 9a**), and MRC1 (mannose receptor C-type 1, **Figure 9b**) proteins, which are markers of M1 and M2 macrophage polarization, respectively. The expression of Periostin (**Figure 9c**), which is a protein involved in bone regeneration via periosteal stem cells, was also investigated. At 6 d, examination of the soft tissues interposed between the implant and bone indicated that inflammatory cells that were positive to iNOS were present in the dCMC group, and to a lesser extent in the PCU, CaP, and Sham groups. In support of these observations, the quantification of iNOS-positive cells was higher in the dCMC group in comparison to PCU and Sham groups (**Figure 9d**). At 28 d, the expression of iNOS decreased in dCMC without differences between groups in the expression of any of the studied proteins. No significant differences in the proportion of MRC1-positive cells were found between the different implant types at 6 d and 28 d. Moreover, the histochemical analysis using Tartrate-resistant acid phosphatase (TRAP) to detect osteoclasts (**Figure S6**) did not exhibit evident reactivity on the surface of bones adjoining the implants at 6 d and 28 d suggesting that bone remodelling activities were not activated in any of the groups.

Together, the PCU membranes, either alone or in combination with dCMC or CaP, were surrounded by a fibrous capsule without direct contact with bone. Compared with the other groups, the dCMC group appeared more associated with cells exhibiting an inflammatory phenotype in the peri-implant tissues.

4. Discussion

The biocompatibility of polyurethanes in general, and polycarbonate urethane in particular, has been traditionally inferred from long-term morphological studies in animal models (*25, 26*) or humans *(27, 28)*, and from cytocompatibility assays *in vitro (29)*. The present study reinforces the understanding of PCU biocompatibility, providing insights about the cellular and molecular mechanisms that drive the *in vivo* response to this biomaterial. PCU implants with or without coatings are shown to elicit an initial inflammatory response that subsequently resolves in a relatively thin, proper soft tissue encapsulation both in soft tissue and in contact with bone.

In a study that used the same animal model as herein, polyurethane urea—another variant of polyurethane elastomer—was previously proven *(30)* to exhibit comparable biocompatibility to titanium, which is widely acknowledged as a state-of-the-art biocompatible metallic biomaterial. Interaction with polyurethane urea implants resulted in a decreased inflammatory response and a lower secretion of the proinflammatory cytokine TNF during the early postoperative phase compared to titanium implants. Furthermore, polyurethane urea implants were associated with increased secretion of the anti-inflammatory cytokine IL-10 and a heightened presence of pro-regenerative macrophages at the implant interface. Importantly, no significant differences were observed in the levels of the cytotoxic marker LDH when compared to those in Sham controls (*30*). The response elicited by PCU in the present study recapitulates several key characteristics that were observed with polyurethane urea implants, highlighting its biocompatibility. Beyond the comparable levels of LDH, PCU implants showed no significant differences in cell counts or in the expression of genes associated with inflammatory cytokines or macrophage polarization in comparison to Sham sites. PCU effectively mitigated the initial inflammatory response and promoted the expression of the reparative gene *TGFβ* as early as 3 d post-implantation. As a result, the fibrous capsule surrounding the PCU implants was thicker than that around the other implants in this study. Yet, this thickness aligns with that of peri-implant capsules with other biomaterials such as titanium (*31*) or magnesium (*24*), which have been demonstrated to possess biocompatible properties in the same soft tissue model.

Moreover, in the present study, the CaP group mirrored most of the primary findings observed during the inflammatory and reparative phases in both the PCU and Sham groups. These results are consistent with previous *in vivo* (*32*) and *in vitro* (*33*) studies that showed the biocompatibility of CaP coatings (*34*). For instance, the subcutaneous implantation of CaP-coated titanium discs in goats (*35*) resulted in a fibrous encapsulation comparable to that around uncoated titanium implants over a period of 2 to 12 w, without discernible adverse effects. Furthermore, previous *in vitro* tests of PCU and CaP-coated PCU (*21*), which were identical to those employed in the present study, demonstrated comparable viability and differentiation of human bone marrow mesenchymal stem cells. The CaP coating on PCU was revealed to be amorphous in the present study. Intriguingly, compared to uncoated titanium implants, this specific CaP phase on the surface of titanium implants has been shown to decrease

chemotaxis to the implants and reduce cytotoxicity during the postoperative period in the same rat soft tissue model as in the present study (*36*), further supporting the biocompatibility of CaP-coated PCU.

A major finding in this study was the distinct initial response to dCMC-coated PCU, which was characterized by increased inflammation, neoangiogenesis, and apoptosis. Indicative of the early activation of proinflammatory pathways, the present study provides the first *in vivo* evidence of the ability of dopamine-carboxymethyl cellulose conjugates to strongly stimulate M1 macrophage-related gene expression. Dopamine is a critical catecholamine neurotransmitter (*37*) expressed by several immune cells and plays an important role in cell-cell communication during the immune response. For example, dopamine produced by dendritic cells amplifies inflammation by activating the response of Th17 cells (*38*). Moreover, dopamine has been previously associated with the proinflammatory activation of microglia, the brain-resident macrophages (*39*). In response to dopamine, microglia exhibited increased cellular migration along with heightened secretion of nitric oxide and proinflammatory cytokines, which are characteristic of the M1 phenotype, in cell culture and tissue sections of rodents (*39*). Similarly, dopamine administration was proven to polarize tumor-associated macrophages toward the M1 phenotype, thus inhibiting tumor growth in a rat glioma model (*40*). While coactivation of proinflammatory macrophage and neoangiogenesis pathways, as observed in the dCMC group is widely established in biomaterial-associated responses (*41*), questions remain about the elevated cytotoxicity in this group. Beyond the potential concentration-dependent toxicity of dopamine, these questions might hypothetically be answered by the synergistic association between nitric oxide-mediated oxidative stress and dopamine-induced mitochondrial dysfunction, both of which are known to have cytotoxic implications (*42*). A role of carboxymethyl cellulose in promoting cell death appears less likely, given the strong evidence that negates the cytotoxic effects of this cellulose derivative. However, its potential impact on the initial response to dCMC should not be entirely dismissed, considering recent findings demonstrating its ability to significantly modulate the cellular metabolism (*43*) in general, and inflammation (*44*) in particular. In fact, *in vitro* studies (*44*) have shown that carboxymethyl cellulose can modulate the macrophage inflammatory response by simultaneously stimulating both proinflammatory (TNF and MCP1) and anti-inflammatory (IL10) cytokines. This duality mirrors the findings in the dCMC group of the current study, particularly in terms of the qPCR results of implant-adherent cells. However, it is intriguing that this concomitant activation of M1 and M2 macrophage gene markers at the implant surface in the dCMC group was not replicated in the surrounding exudate, revealing specific activation of macrophage programs. This discrepancy between gene expression at the implant surface and the peri-implant exudate raises questions about the potential role of PCU in modulating the initial proinflammatory reaction to dCMC. Therefore, delineating the specific contributions of dopamine, carboxymethyl cellulose, and PCU to the initial response in the dCMC group warrants further elucidation.

In all the experimental groups, the initial inflammatory response was effectively alleviated, facilitating reparative encapsulation of the implants in soft tissue. However, in bone, none of the experimental treatments, including CaP-coated PCU, achieved direct bone contact despite the ability to promote mesenchymal stem cell differentiation toward the osteogenic lineage *in vitro* (*21*). The osteogenic differentiation of skeletal stem/progenitor cells, predominantly originating from the bone marrow and the periosteum is a pivotal factor in bone formation (*45, 46*). In the present study, these cells could not be derived from the bone marrow compartment upon preservation of the continuity of the cortical barrier, nor could they come from the periosteum due to surgical release (*47*). The surrounding skeletal muscles, although also capable of furnishing osteoprogenitors (*48*), supply nutrients via vascular ingrowth, which is vital for the repair of the injured bone (*49*). The obstruction of vascular invasion by interposition of the foil between the injured bone and surrounding muscles (*49*) in this study further diminished the osteogenic potential at the operated sites. This was evidenced not only by the low detection of Periostin, which is a crucial factor for bone regeneration in the injured periosteum (*46*), but also by the consistent fibrous encapsulation of the implants.

In agreement with standardized, experimental biocompatibility protocols, the present study utilized normal tissue conditions. However, this study does not address the biocompatibility of the studied materials in an inflammatory environment with a constitutively increased expression of proinflammatory and tissue-degrading molecules due to disease. Similarly, the interactions between the selected materials and the variability of the surface structure/texture of cartilage and bone surfaces inside small joints affected by OA were not studied. Moreover, the experimental models used in the present study do not allow the investigation of the influence of the implants on pain elicited by OA. These obvious limitations require further interrogation in a real-life, osteoarthritic joint milieu, which would be an important step in the clinical translation of this concept. Furthermore, the polymer foil inside a joint would be subjected to cyclic loads during joint motion, eventually leading to the generation of wear particles that may potentially accumulate over time. While the surface treatment within the implant is designed to minimize wear, released particles are expected to be contained inside the implant. Beyond the need to determine the long-term biological response to the implants, future studies require a focus on the eventual release of abraded particles under mechanical load in the joint by characterizing their type, quantity, size, and shape.

In the context of hand OA, which is characterized by a lack of skeletal stem/progenitor cells from the periosteum or muscles, achieving the integration of PCU membranes in subchondral bone with or without coatings is less likely. The present findings prompt a consideration of the necessity for mechanical fixation of these membranes to bone surfaces (*18*) in the context of the APRICOT implants. Nevertheless, proper fibrous encapsulation of PCU membranes could play a crucial role in stabilizing APRICOT® implants. This concept is reminiscent of the Swanson-hinged silicone joint

spacer that is widely used in hand OA surgery (*11, 50*). In addition to supporting the surrounding synovial capsule and alleviating pain, the fibrous encapsulation of these implants is believed to avoid the need for permanent implant transfixation in bone, thereby potentially extending the lifespan of the implant (*11*). Although the conditions of hand OA are not replicated in the animal models that were used in this study, these models are instrumental for delineating the responses of various cell types to the implants. In the soft tissue model, the distinct compartmentalization of the soft tissue–implant interfaces enabled a comprehensive characterization of cellular behavior and distribution. In bone, the response of skeletal cells to the implants facilitated an assessment of the local response and adaptation of the membranes while excluding potent periosteal osteoprogenitors. These findings are relevant to the biocompatibility of the APRICOT® implants, as well as their capacity for bone integration, and provide crucial insights to establishing a proof-of-concept for human applications.

5. Conclusion

For the first time, this study used cellular and molecular analyses to investigate the *in vivo* response of cells at the interface with native and surface-modified PCU implants. A transient initial inflammation followed by reparative fibrous encapsulation was found to be consistent across all implant groups, regardless surface modification. However, PCU surfaces functionalized with dCMC initially exhibited evident M1 macrophage-driven exacerbation of inflammation with diminished viability and proapoptotic gene expression of the recruited cells. While reparative osteogenesis via Periostin was not observed at the implant–bone interface, a fibrous encapsulation of all the implants without a protracted inflammation demonstrated a proper adaptation to the bone surface. Based on these experimental observations, it is concluded that PCU and CaP-coated PCU foils are candidate biomaterials for the application of the APRICOT® concept in small finger joints.

6. References

1. C. f. D. Control, Prevention, Prevalence and most common causes of disability among adults--United States, 2005. *MMWR Morb Mortal Wkly Rep* **58**, 421-426 (2009).
2. M. Marshall, F. E. Watt, T. L. Vincent, K. Dziedzic, Hand osteoarthritis: clinical phenotypes, molecular mechanisms and disease management. *Nat Rev Rheumatol* **14**, 641-656 (2018).
3. M. B. Goldring, S. R. Goldring, Osteoarthritis. *J. Cell. Physiol.* **213**, 626-634 (2007).
4. Y. Wang, G. Jones, H. I. Keen, C. L. Hill, A. E. Wluka, J. Kasza, A. J. Teichtahl, B. Antony, R. O'Sullivan, F. M. Cicuttini, Methotrexate to treat hand osteoarthritis with synovitis (METHODS): an Australian, multisite, parallel-group, double-blind, randomised, placebo-controlled trial. *Lancet* **402**, 1764-1772 (2023).
5. F. Kroon, M. Kortekaas, A. Boonen, S. Böhringer, M. Reijnierse, F. Rosendaal, N. Riyazi, M. Starmans, F. Turkstra, J. van Zeben, Results of a 6-week treatment with 10 mg prednisolone in patients with hand osteoarthritis (HOPE): a double-blind, randomised, placebo-controlled trial. *Lancet* **394**, 1993-2001 (2019).
6. M. Kloppenburg, Hand osteoarthritis-nonpharmacological and pharmacological treatments. *Nat Rev Rheumatol* **10**, 242-251 (2014).

7. M. Kloppenburg, F. P. Kroon, F. J. Blanco, M. Doherty, K. S. Dziedzic, E. Greibrokk, I. K. Haugen, G. Herrero-Beaumont, H. Jonsson, I. Kjeken, E. Maheu, R. Ramonda, M. J. Ritt, W. Smeets, J. S. Smolen, T. A. Stamm, Z. Szekanecz, R. Wittoek, L. Carmona, 2018 update of the EULAR recommendations for the management of hand osteoarthritis. *Ann Rheum Dis* **78**, 16-24 (2019).
8. D. B. Herren, H. Ishikawa, M. Rizzo, M. Ross, M. Solomons, Arthroplasty in the hand: what works and what doesn't? *J Hand Surg Eur Vol* **47**, 4-11 (2022).
9. J. J. Srnec, E. R. Wagner, M. Rizzo, Implant Arthroplasty for Proximal Interphalangeal, Metacarpophalangeal, and Trapeziometacarpal Joint Degeneration. *J Hand Surg Am* **42**, 817-825 (2017).
10. A. B. Swanson, Flexible implant resection arthroplasty. *Hand* **4**, 119-134 (1972).
11. D. H. DeHeer, S. R. Owens, A. B. Swanson, The host response to silicone elastomer implants for small joint arthroplasty. *J Hand Surg Am* **20**, S101-109 (1995).
12. S. L. Moran, M. Rizzo, Managing Difficult Problems in Small Joint Arthroplasty: Challenges, Complications, and Revisions. *Hand Clin* **39**, 307-320 (2023).
13. J. Adams, C. Ryall, A. Pandyan, C. Metcalf, M. Stokes, S. Bradley, D. J. Warwick, Proximal interphalangeal joint replacement in patients with arthritis of the hand: a meta-analysis. *J Bone Joint Surg Br* **94**, 1305-1312 (2012).
14. J. I. Billig, J. S. Nasser, K. C. Chung, National Prevalence of Complications and Cost of Small Joint Arthroplasty for Hand Osteoarthritis and Post-Traumatic Arthritis. *J. Hand Surg. Am.* **45**, 553 e551-553 e512 (2020).
15. R. L. Linscheid, Implant arthroplasty of the hand: retrospective and prospective considerations. *J. Hand Surg. Am.* **25**, 796-816 (2000).
16. A. C. Taylor. (2021), chap. WO2021/111107.
17. M. Shemesh, A. Shefy-Peleg, A. Levy, N. Shabshin, V. Condello, R. Arbel, A. Gefen, Effects of a novel medial meniscus implant on the knee compartments: imaging and biomechanical aspects. *Biomech. Model. Mechanobiol.* **19**, 2049-2059 (2020).
18. P. Farjam, E. E. G. Hekman, J. Rouwkema, G. J. Verkerke, Bone fixation techniques for managing joint disorders and injuries: A review study. *J. Mech. Behav. Biomed. Mater.* **126**, 104982 (2022).
19. D. J. Hunter, S. Bierma-Zeinstra, Osteoarthritis. *Lancet* **393**, 1745-1759 (2019).
20. S. Pan, Y. Li, X. Tong, L. Chen, L. Wang, T. Li, Q. Zhang, Strongly-adhesive easily-detachable carboxymethyl cellulose aerogel for noncompressible hemorrhage control. *Carbohydrate Polymers* **301**, 120324-120324 (2023).
21. P. Farjam, M. Luckabauer, E. de Vries, V. Rangel, E. Hekman, G. Verkerke, J. Rouwkema, Bioactive calcium phosphate coatings applied to flexible poly (carbonate urethane) foils. *Surf Coat Technol* **470**, 129838 (2023).
22. F. Suska, M. Esposito, C. Gretzer, M. Källtorp, P. Tengvall, P. Thomsen, IL-1α, IL-1β and TNF-α secretion during in vivo/ex vivo cellular interactions with titanium and copper. *Biomaterials* **24**, 461-468 (2003).
23. S. Svensson, M. Trobos, M. Hoffman, B. Norlindh, S. Petronis, J. Lausmaa, F. Suska, P. Thomsen, A novel soft tissue model for biomaterial-associated infection and inflammation - bacteriological, morphological and molecular observations. *Biomaterials* **41**, 106-121 (2015).
24. H. Ben Amara, D. C. Martinez, F. A. Shah, A. J. Loo, L. Emanuelsson, B. Norlindh, R. Willumeit-Romer, T. Plocinski, W. Swieszkowski, A. Palmquist, O. Omar, P. Thomsen, Magnesium implant degradation provides immunomodulatory and proangiogenic effects and attenuates peri-implant fibrosis in soft tissues. *Bioact Mater* **26**, 353-369 (2023).
25. A. B. Mathur, T. O. Collier, W. J. Kao, M. Wiggins, M. A. Schubert, A. Hiltner, J. M. Anderson, In vivo biocompatibility and biostability of modified polyurethanes. *J. Biomed. Mater. Res.* **36**, 246-257 (1997).

26. W. K. Ward, E. P. Slobodzian, K. L. Tiekotter, M. D. Wood, The effect of microgeometry, implant thickness and polyurethane chemistry on the foreign body response to subcutaneous implants. *Biomaterials* **23**, 4185-4192 (2002).
27. M. Esposito, C. Kennergren, N. Holmstrom, S. Nilsson, J. Eckerdal, P. Thomsen, Morphologic and immunohistochemical observations of tissues surrounding retrieved transvenous pacemaker leads. *J Biomed Mater Res* **63**, 548-558 (2002).
28. J. Frame, D. Kamel, M. Olivan, H. Cintra, The In Vivo Pericapsular Tissue Response to Modern Polyurethane Breast Implants. *Aesthetic Plast Surg* **39**, 713-723 (2015).
29. J. A. Jones, M. Dadsetan, T. O. Collier, M. Ebert, K. S. Stokes, R. S. Ward, P. A. Hiltner, J. M. Anderson, Macrophage behavior on surface-modified polyurethanes. *J Biomater Sci Polym Ed* **15**, 567-584 (2004).
30. C. Gretzer, L. Emanuelsson, E. Liljensten, P. Thomsen, The inflammatory cell influx and cytokines changes during transition from acute inflammation to fibrous repair around implanted materials. *J Biomater Sci Polym Ed* **17**, 669-687 (2006).
31. F. Suska, L. Emanuelsson, A. Johansson, P. Tengvall, P. Thomsen, Fibrous capsule formation around titanium and copper. *J. Biomed. Mater. Res. A* **85**, 888-896 (2008).
32. S. Mohammadi, M. Esposito, J. Hall, L. Emanuelsson, A. Krozer, P. Thomsen, Long-term bone response to titanium implants coated with thin radiofrequent magnetron-sputtered hydroxyapatite in rabbits. *Int J Oral Maxillofac Implants* **19**, 498-509 (2004).
33. L. Ryden, O. Omar, A. Johansson, R. Jimbo, A. Palmquist, P. Thomsen, Inflammatory cell response to ultra-thin amorphous and crystalline hydroxyapatite surfaces. *J Mater Sci Mater Med* **28**, 9 (2017).
34. S. R. Paital, N. B. Dahotre, Calcium phosphate coatings for bio-implant applications: Materials, performance factors, and methodologies. *Materials Science and Engineering: R: Reports* **66**, 1-70 (2009).
35. S. C. Leeuwenburgh, J. G. Wolke, M. C. Siebers, J. Schoonman, J. A. Jansen, In vitro and in vivo reactivity of porous, electrosprayed calcium phosphate coatings. *Biomaterials* **27**, 3368-3378 (2006).
36. L. Ryden, D. Molnar, M. Esposito, A. Johansson, F. Suska, A. Palmquist, P. Thomsen, Early inflammatory response in soft tissues induced by thin calcium phosphates. *J Biomed Mater Res A* **101**, 2712-2717 (2013).
37. S. Paravati, A. Rosani, S. J. Warrington, "Physiology, Catecholamines" (StatPearls Publishing, 2023).
38. R. Pacheco, F. Contreras, M. Zouali, The dopaminergic system in autoimmune diseases. *Front Immunol* 5, 117 (2014).
39. K. Farber, U. Pannasch, H. Kettenmann, Dopamine and noradrenaline control distinct functions in rodent microglial cells. *Mol Cell Neurosci* **29**, 128-138 (2005).
40. T. Qin, C. Wang, X. Chen, C. Duan, X. Zhang, J. Zhang, H. Chai, T. Tang, H. Chen, J. Yue, Dopamine induces growth inhibition and vascular normalization through reprogramming M2-polarized macrophages in rat C6 glioma. *Toxicol Appl Pharmacol* **286**, 112-123 (2015).
41. R. Whitaker, B. Hernaez-Estrada, R. M. Hernandez, E. Santos-Vizcaino, K. L. Spiller, Immunomodulatory biomaterials for tissue repair. *Chem. Rev.* **121**, 11305-11335 (2021).
42. C. Nunes, J. Laranjinha, Nitric oxide and dopamine metabolism converge via mitochondrial dysfunction in the mechanisms of neurodegeneration in Parkinson's disease. *Arch. Biochem. Biophys.* **704**, 108877 (2021).
43. A. Baran, E. Sulukan, M. Türkoğlu, A. Ghosigharehagaji, S. Yildirim, M. Kankaynar, I. Bolat, M. Kaya, A. Topal, S. B. Ceyhun, Is sodium carboxymethyl cellulose (CMC) really completely innocent? It may be triggering obesity. *Int J Biol Macromol* **163**, 2465-2473 (2020).

44. E. M. Costa, S. Silva, C. F. Pereira, A. B. Ribeiro, F. Casanova, R. Freixo, M. Pintado, Ó. L. Ramos, Carboxymethyl Cellulose as a Food Emulsifier: Are Its Days Numbered? *Polymers* **15**, 2408 (2023).
45. S. Perrin, C. Colnot, Periosteal Skeletal Stem and Progenitor Cells in Bone Regeneration. *Curr Osteoporos Rep* **20**, 334-343 (2022).
46. O. Duchamp de Lageneste, A. Julien, R. Abou-Khalil, G. Frangi, C. Carvalho, N. Cagnard, C. Cordier, S. J. Conway, C. Colnot, Periosteum contains skeletal stem cells with high bone regenerative potential controlled by Periostin. *Nat Commun* **9**, 773 (2018).
47. P. Garcia, J. H. Holstein, S. Maier, H. Schaumloffel, F. Al-Marrawi, M. Hannig, T. Pohlemann, M. D. Menger, Development of a reliable non-union model in mice. *J Surg Res* **147**, 84-91 (2008).
48. A. Julien, A. Kanagalingam, E. Martinez-Sarra, J. Megret, M. Luka, M. Menager, F. Relaix, C. Colnot, Direct contribution of skeletal muscle mesenchymal progenitors to bone repair. *Nat Commun* **12**, 2860 (2021).
49. N. van Gastel, S. Stegen, G. Eelen, S. Schoors, A. Carlier, V. W. Daniels, N. Baryawno, D. Przybylski, M. Depypere, P. J. Stiers, D. Lambrechts, R. Van Looveren, S. Torrekens, A. Sharda, P. Agostinis, D. Lambrechts, F. Maes, J. V. Swinnen, L. Geris, H. Van Oosterwyck, B. Thienpont, P. Carmeliet, D. T. Scadden, G. Carmeliet, Lipid availability determines fate of skeletal progenitor cells via SOX9. *Nature* **579**, 111-117 (2020).
50. A. B. Swanson, G. de Groot Swanson, Flexible implant resection arthroplasty for the rheumatoid hand and wrist. *Ann. Chir. Gynaecol. Suppl.* **198**, 54-69 (1985).

Acknowledgments

The assistance of Lena Emanuelsson, Birgitta Norlindh and Anna Johansson during the *in vivo* experiments, morphological and immunohistochemical preparation, sectioning steps, and qPCR analyses is greatly appreciated. Financial support was received from the European Union's Horizon 2020 Research and Innovation Programme under grant agreement No 863183, the Swedish state under the agreement between the Swedish government and the county councils, the ALF agreement (ALFGBG-725641), the IngaBritt and Arne Lundberg Foundation; the Sylvan Foundation, and the Area of Advance Materials of Chalmers and GU Biomaterials within the Strategic Research Area Initiative launched by the Swedish government. The funding sources played no role in the study conceptualization, study design, data collection, data analysis, decision to publish, or preparation of the manuscript. “BioRender.com” was used for the illustrations.

Declaration of conflicts of interest

Andy Taylor is the inventor and holds patents related to the device. The other authors do not have any conflict of interest to declare.

Figure legends

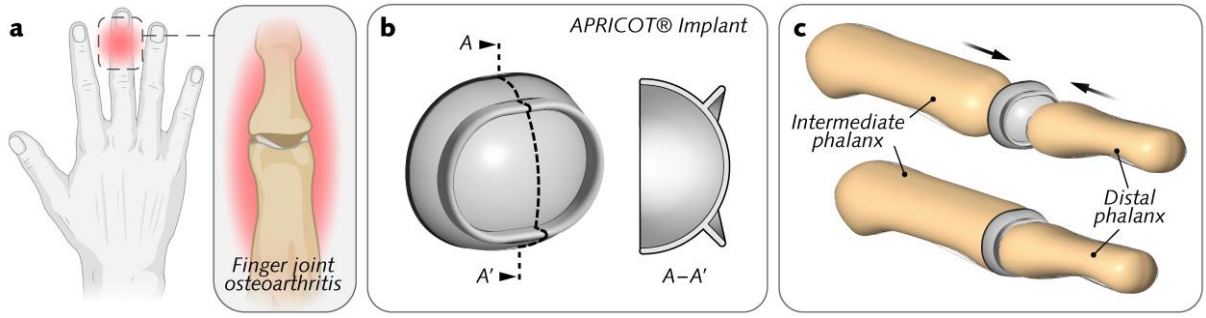

Figure 1: **The APRICOT® implant for hand osteoarthritis**
(**a**), Hand affected by osteoarthritis with diseased tissues in the finger joint. (**b**), The APRICOT® implant, shown in a 3D representation and in a cross-sectional view (A-A'), is designed to conform to the contour of the diseased joint. (**c**), Installation of the APRICOT® implant in the distal interphalangeal joint of a hand finger. Illustrations in **b** and **c** are adapted from (*16*).

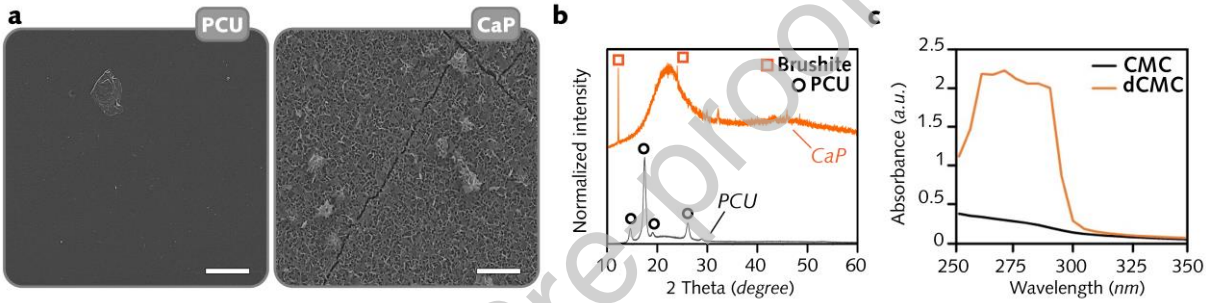

Figure 2: **Material characterization**
(**a**), Scanning electron micrographs of bare polycarbonate urethane (PCU) and PCU coated with a layer of calcium phosphate (CaP). (**b**), XRD pattern of the bare PCU film and the PCU film coated with CaP. (**c**), Successful conjugation of dopamine to carboxymethylcellulose was verified by detecting a strong absorbance peak obtained at 280 nm. Scale bar: **a** = 5 µm.

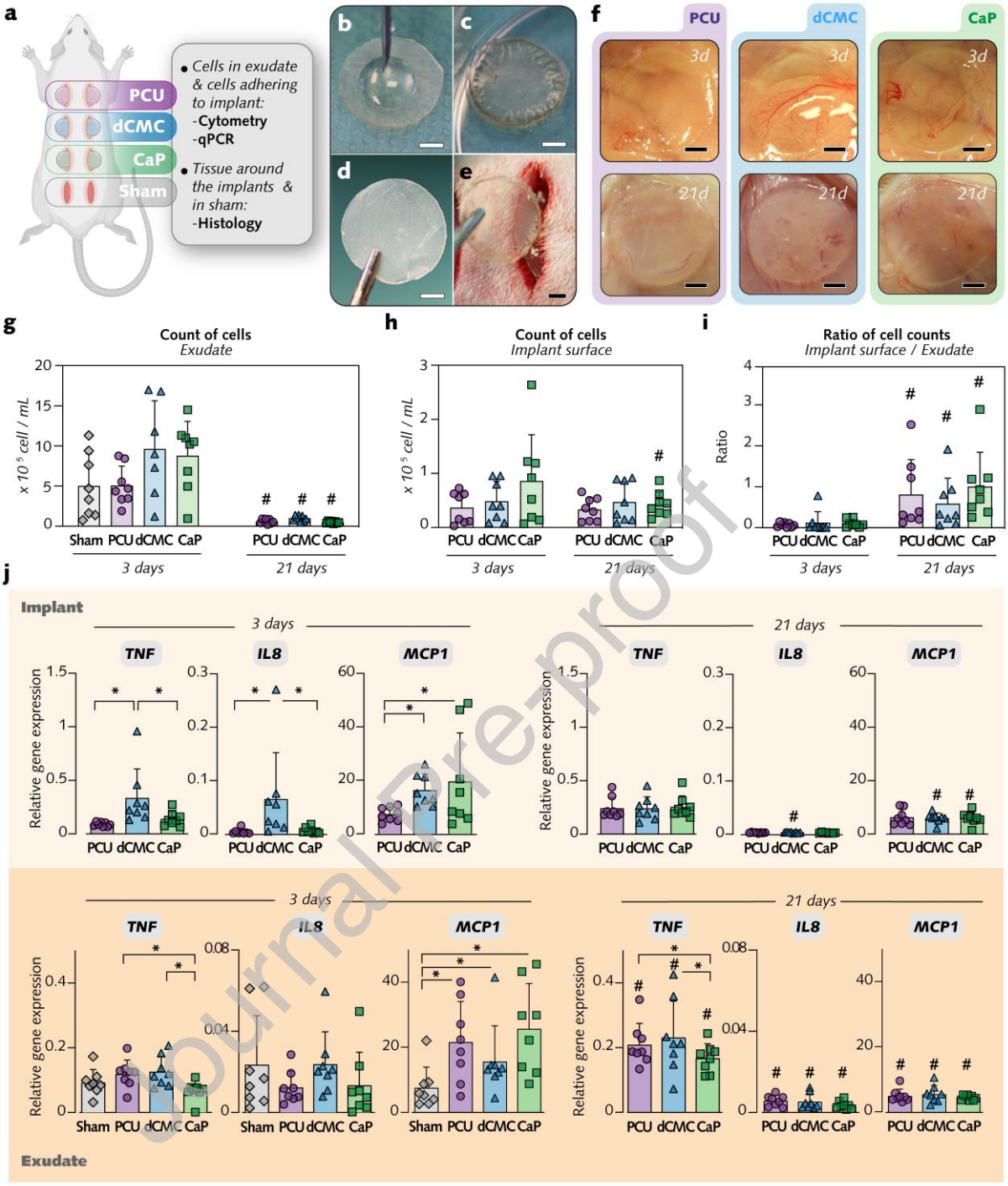

Figure 3: **Implants in soft tissue promote transient cellular migration and upregulation of inflammatory cytokines and chemokines**

(**a-c**), Disc-shaped implants made of polycarbonate urethane (PCU) with a dopamine-carboxymethylcellulose film (dCMC) applied upon hydration (**b**, **c**) or coated with a calcium phosphate layer (CaP; **d**) were subcutaneously inserted into the dorsum of rats (**e**, **a**) according to a randomization scheme. In addition to those from the Sham sites, the implants with or without surrounding tissue were retrieved after 3 d and 21 d. Analyses of cells that adhered to the implants, those in the per-implant exudate, or those in the Sham exudate were analyzed via cytometry and gene expression assays (no exudate was collected from the Sham group at 21 d due to the closure of the pockets). Tissues around the implants or those retrieved from the

Sham group were examined via histology. (**g-i**), Total cells from the implant surface (**g**) and from the exudate (**h**) were counted separately and the corresponding ratio of *implant surface/exudate* cell counts was determined (**i**) (n = 8/group/timepoint). (**j**), qPCR analysis of the relative mRNA levels of inflammatory markers (*TNF, IL8,* and *MCP1)* at the implant surface (*top panel*) and in the exudate (*bottom panel*) (n = 8/group/timepoint).
The data are shown as the mean ± s.d. * $P<0.05$ PCU *versus* dCMC *versus* CaP *versus* Sham. # $P<0.05$ 3 d *versus* 21 d. Kruskal–Wallis and two-way ANOVA tests were performed. Scale bars: **b-f** = 2 mm.

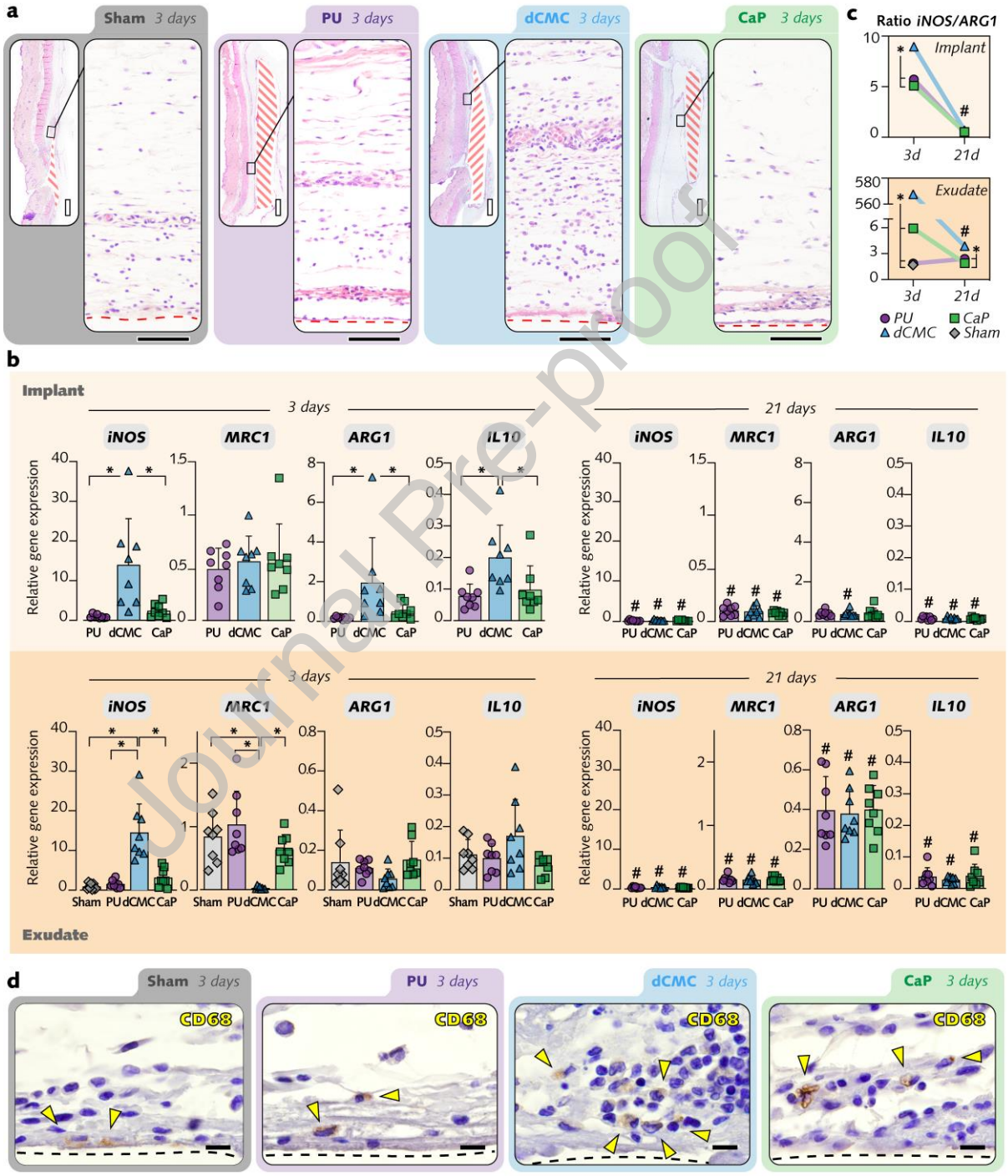

Figure 4: **Initial cellular infiltration of peri-implant tissues and regulation of genes related to macrophage polarization**

(**a**), Histology of implants and the associated tissues and Sham tissues at 3 d. Areas outlined in dashed red lines indicate the implants. The dashed red lines show the implant–tissue interface. Hematoxylin and eosin staining (**b**), qPCR analysis of the relative mRNA levels of macrophage markers (*iNOS, MRC1, ARG1* and *IL10*) at the implant surface and in the exudate (n = 8/group/timepoint). (**c**), The ratio of *iNOS/ARG1* mRNA levels indicates the proportions of proinflammatory macrophages (M1) *versus* proregenerative macrophages (M2) among cells that adhered to the implant surface (*top panel*) or among cells in the exudate (*bottom panel*) (one mean value representing n = 8/group/timepoint; details in Figure S1). (**d**), Immunohistochemistry to detect CD68-positive cells (arrowheads) at 3 d in soft tissue sections (CD68-immunohistochemistry in the 21 d-soft tissue sections is shown in Figure S4). Dashed lines indicate soft tissue–implant interface.

The data are shown as the mean ± s.d. * $P<0.05$ PCU *versus* dCMC *versus* CaP *versus* Sham. # $P<0.05$ 3 d *versus* 21 d. Two-way ANOVA. Scale bars: **a**: *white* = 1 mm, *black* = 100 µm, **d** = 5 µm.

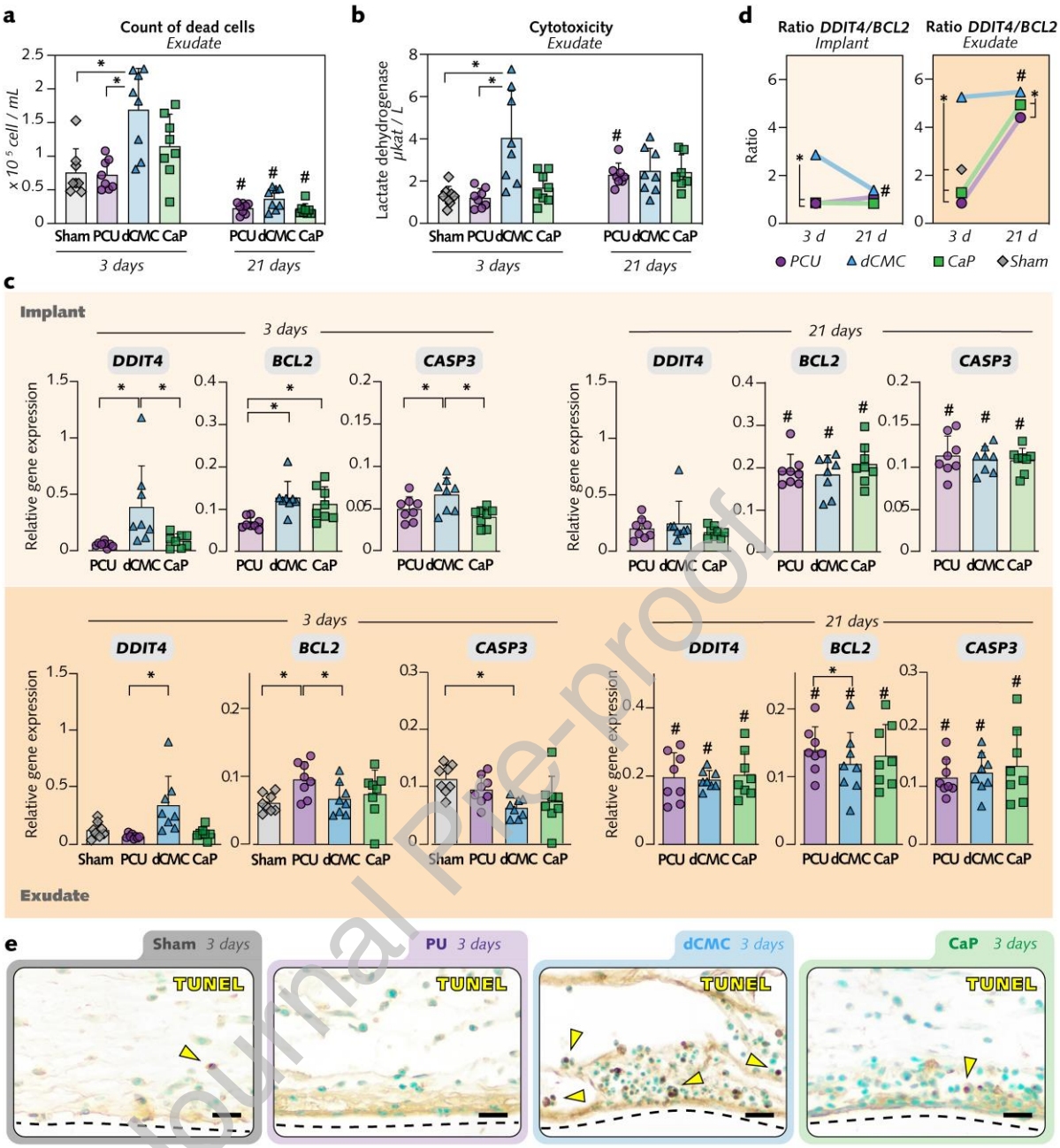

Figure 5: **Cell viability, cytotoxicity, and regulation of genes related to apoptosis-related pathways**

(**a-b**), In the exudates, the number of dead cells (**a**) and the lactate dehydrogenase (LDH) concentration (cytotoxicity; **b**) were measured (n = 8/group/timepoint). qPCR (**c**) analyzed the relative mRNA levels of apoptotic (*DDIT4* and *CASP3)* and antiapoptotic (*BCL2*) genes at the implant surface and in the exudate (n = 8/group/timepoint). (**d**), Ratio of *DDIT4/BCL2* mRNA levels indicated proapoptotic *versus* antiapoptotic gene expression in cells that adhered to the implant surface (*top panel*) or in cells in the exudate (*bottom panel*) (one mean value represents n = 8/group/timepoint; details in Figure S2). (**e**), Detection of TUNEL-positive cells (arrowheads) indicative of apoptotic cells in soft tissue sections at 3 d (TUNEL histochemistry in 21 d-soft tissue sections are shown in Figure S5). Dashed lines indicate soft tissue–implant interface.

The data are shown as the mean ± s.d. * P<0.05 PCU *versus* dCMC *versus* CaP *versus* Sham. # P<0.05 3 d *versus* 21 d. Kruskal–Wallis and two-way ANOVA tests were used. Scale bar: **e** = 25 µm.

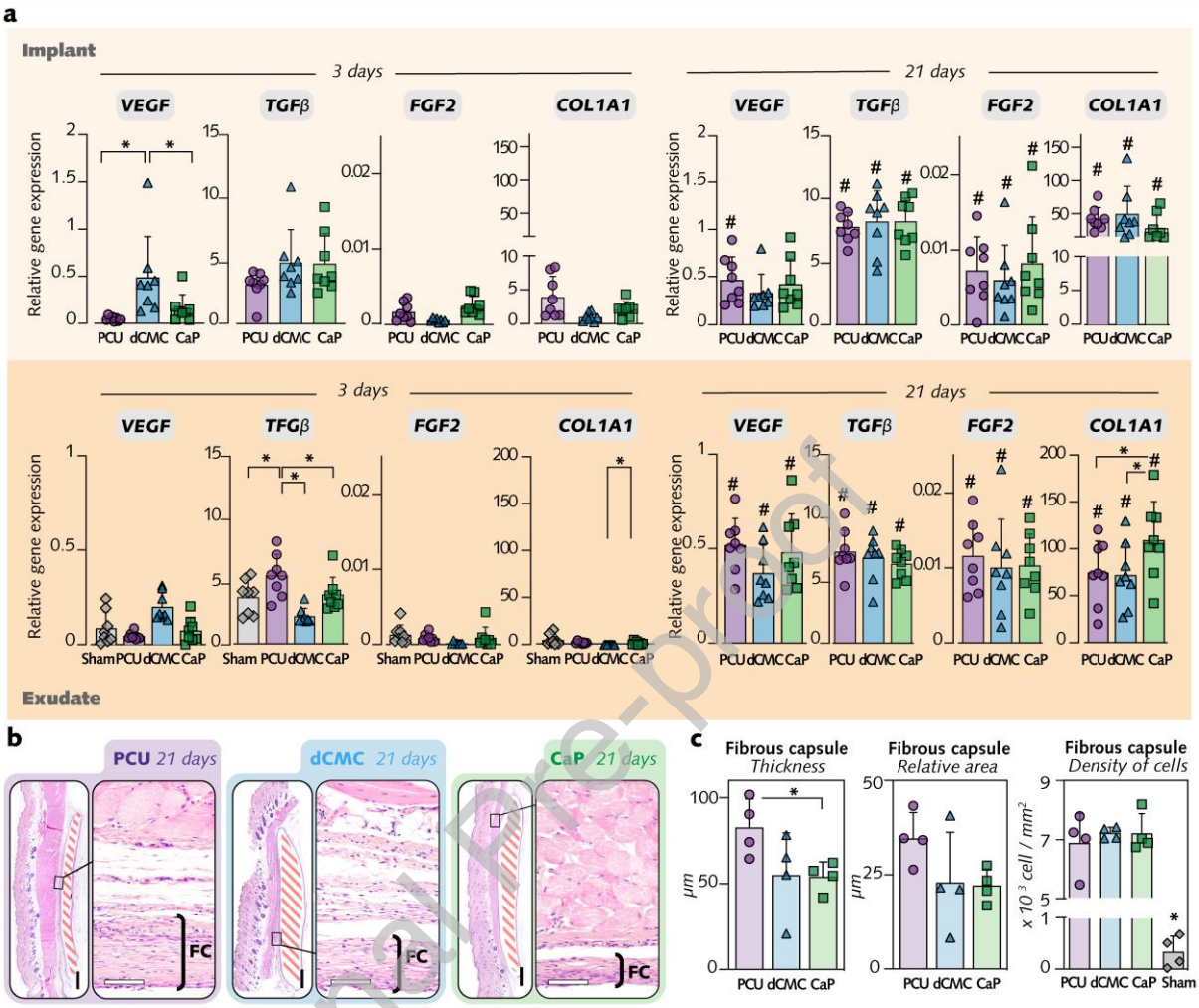

Figure 6: **Fibrous encapsulation and expression of gene markers of regeneration and neoangiogenesis**

(**a**), qPCR analysis of the relative mRNA levels of proregenerative and neoangiogenesis markers at the implant surface and in the exudate (n = 8/group/timepoint). (**b**), Histology of the implant with the associated tissues at 21 d. Areas highlighted in red dashed lines indicate the implants. The peri-implant fibrous capsule (FC) is highlighted. Hematoxylin and eosin staining. (**c**), Histomorphometry of the peri-implant fibrous capsule. The relative area is the area of the capsule normalized to the capsule perimeter (n = 4/group/timepoint).

The data are shown as the mean ± s.d. * P<0.05 PCU *versus* dCMC *versus* CaP *versus* Sham. # P<0.05 3 d *versus* 21 d. Kruskal–Wallis and two-way ANOVA tests were used. Scale bars: **a**: *black* = 1 mm, *white* = 50 µm.

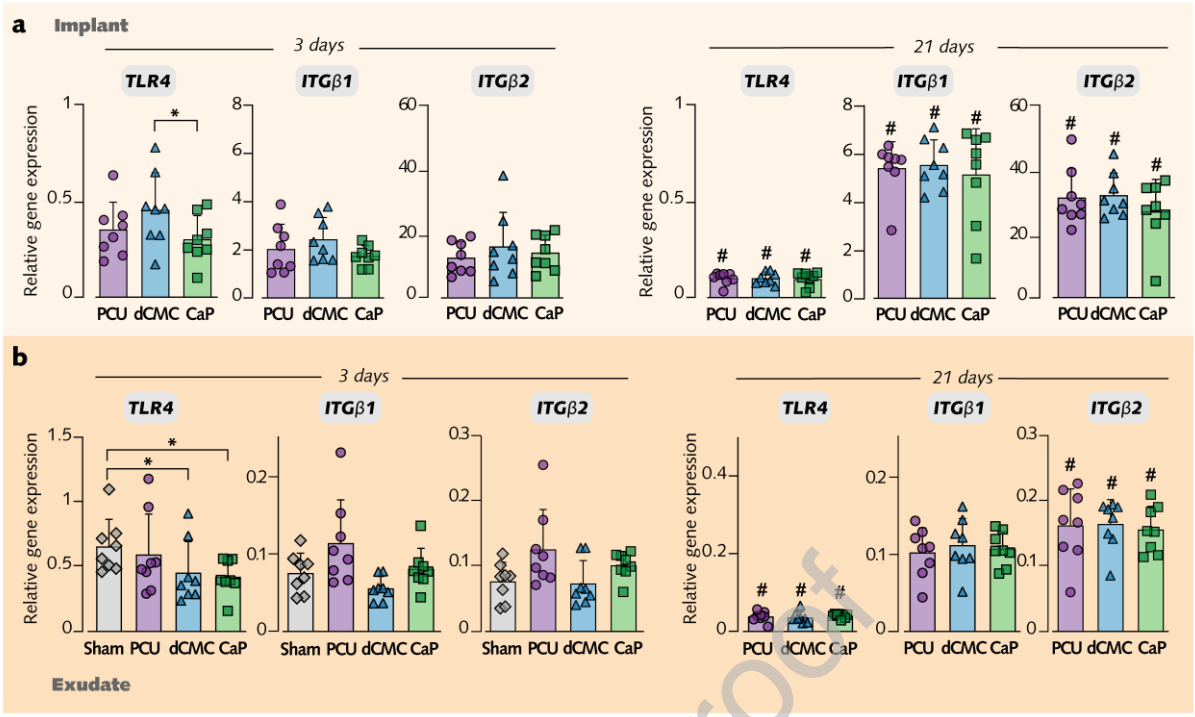

Figure 7: **Regulation of cellular adhesion-related gene expression**
(**a-b**), Relative mRNA levels of cellular adhesion markers (*TLR4. ITGβ1,* and *ITGβ2*) at the implant surface (**a**) and in the exudate (**b**) (n = 8/group/timepoint).
The data are shown as the mean ± s.d. * $P<0.05$ PCU *versus* dCMC *versus* CaP *versus* Sham. # $P<0.05$ 3 d *versus* 21 d. Two-way ANOVA was performed.

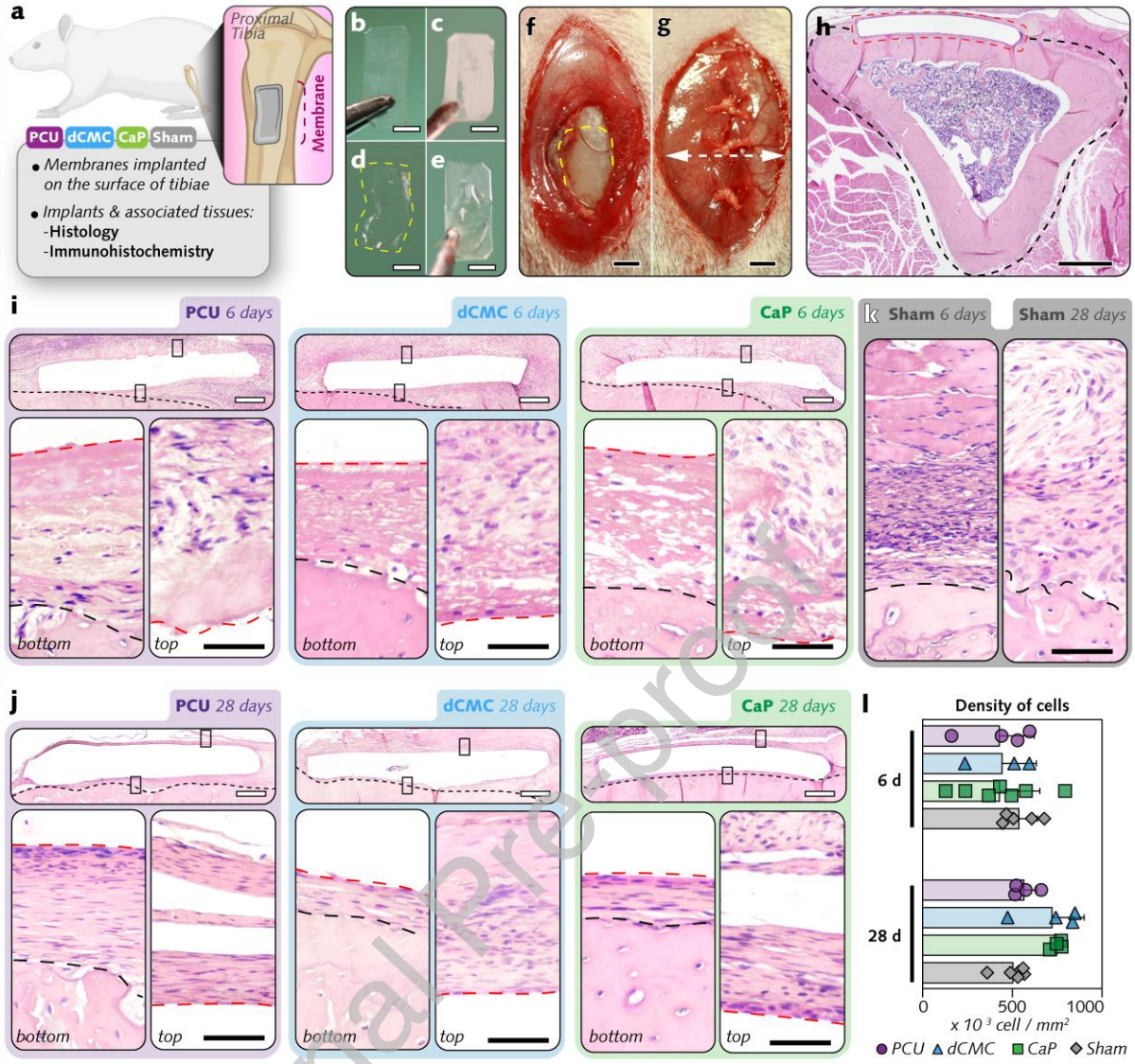

Figure 8: **Bone response to the implants**

(**a-h**), Rectangular membranes (**a**) made of PCU (**b**), coated with CaP (**c**), or with dCMC (**d**) applied upon hydration (**e**) were implanted (**f**) and immobilized (**g**) on the medial surface of the proximal extremity of the tibiae of rats. In addition to Sham sites, implants with surrounding tissue were retrieved after 6 d and 28 d for histological analysis with hematoxylin and eosin (**h**, section from 28 d). Yellow dashed line: dCMC film. White dashed line: axis of histological section of the implants and associated tissues. Red dashed line: implant section. Black dashed line: tibia section. (**i-k**), Histology of the peri-implant soft tissue and bone with magnified tissues interfacing with the top and bottom surface of the implants at 6 d (**i**) and 28 d (**j**), in addition to Sham tissues (**k**). Red dashed line: tissue interfacing with the implant. Black dashed line: junctional region between the bone and the overlaying soft tissue at the surgical site. (**l**), Density of cells in tissues within 100 µm from the implant–tissue interface (n = 3-6/group/timepoint). The data are shown as the mean ± s.d. The Kruskal–Wallis test was used. Scale bars: **b-g** = 2 mm; **h** = 1 mm; **i, j**: *white* = 100 µm, *black* = 50 µm.

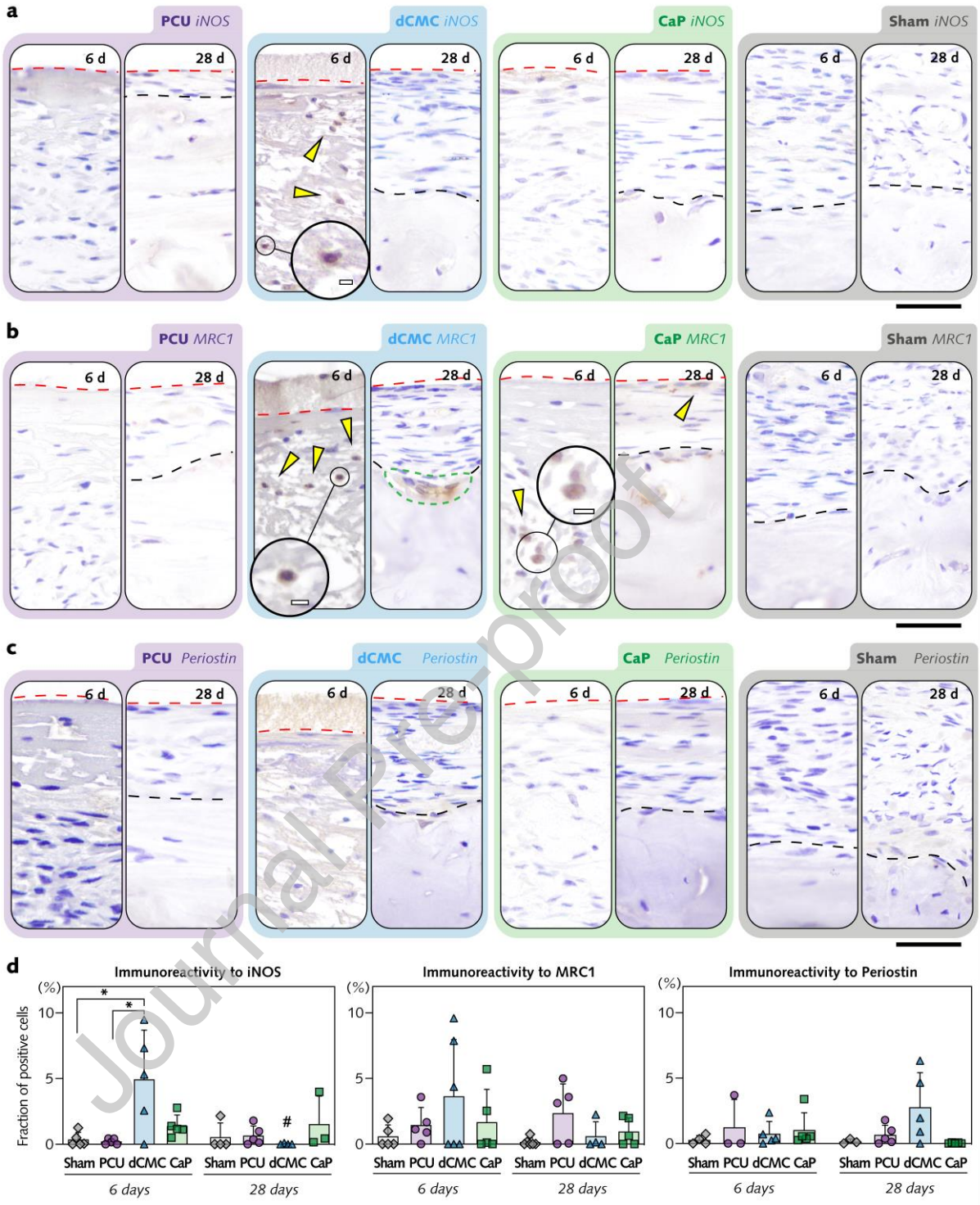

Figure 9: **Immunohistochemistry images of the tissues surrounding the membranes and in Sham sites**

(**a**), Immunohistochemistry to detect iNOS-positive cells at 6 d and 28 d. (**b**), Immunohistochemistry to detect MRC1-positive cells at 6 d and 28 d. (**c**), Immunohistochemistry to detect Periostin-positive cells at 6 d and 28 d. Red dashed line: interface tissue–implant. Black dashed line: the junctional region between the bone and the overlaying soft tissue at the surgical sites. Green dashed line: a multinucleated cell expressing MRC1. Arrowheads and insets highlight immunopositive cells. (**d**), Quantification of cells positive to iNOS, MRC1 and Periostin in tissues within a 100 µm distance from the interface

tissue–implant in PCU, dCMC, and CaP groups and within a 100 μm distance in the soft tissue overlaying bone surface in Sham group (n = 3-6/group/timepoint).
The data are shown as the mean ± s.d. * P<0.05 PCU *versus* dCMC *versus* CaP *versus* Sham. # P<0.05 6 d *versus* 28 d. The Kruskal–Wallis test was used. Scale bars: **a-c**: *black* = 50 μm, *white* = 5 μm.

Graphical Abstract

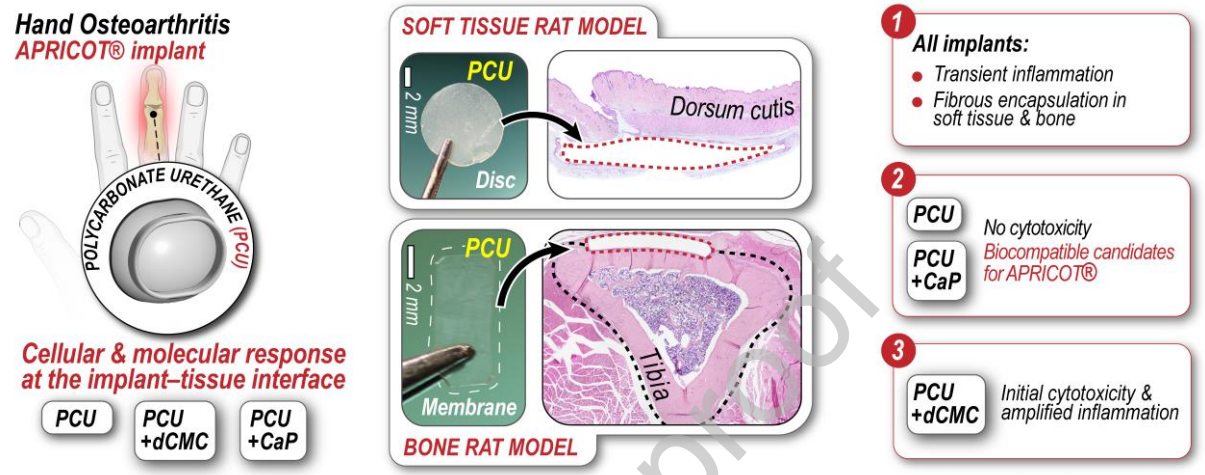

Statement of Significance

Hand osteoarthritis treatments require materials that minimize irritation of the delicate finger joints. Differing from existing treatments, the APRICOT® implant leverages polycarbonate urethane (PCU) for minimally invasive joint replacement. This interdisciplinary, preclinical study investigated the biocompatibility of thin polycarbonate urethane (PCU) foils and their surface modifications with calcium-phosphate (CaP) or dopamine-carboxymethylcellulose (dCMC). Cellular and morphological analyses revealed that both native and Ca-P coated PCU elicit transient inflammation, similar to sham sites, and a thin fibrous encapsulation in soft tissues and on bone surfaces. However, dCMC surface modification amplified initial chemotaxis and cytotoxicity, with pronounced activation of proinflammatory and neoangiogenesis genes. Therefore, native and CaP-coated PCU possess sought-for biocompatible properties, crucial for patient safety and performance of APRICOT® implant.

Declaration of interests

☒ The authors declare that they have no known competing financial interests or personal relationships that could have appeared to influence the work reported in this paper.

☐ The author is an Editorial Board Member/Editor-in-Chief/Associate Editor/Guest Editor for [Journal name] and was not involved in the editorial review or the decision to publish this article.

☒ The authors declare the following financial interests/personal relationships which may be considered as potential competing interests:

Andy Taylor is the inventor and holds patents related to the device. The other authors do not have any conflict of interest to declare.